Supporting Information

Rare-Earth Metal Complexes Bearing an Iminodibenzyl-PNP Pincer Ligand: Synthesis and Reactivity Towards 3,4-Selective Polymerization of 1,3-Dienes

Jingjing Zhai,[a] Fen You,[a] Suting Xu,[a] Ao Zhu,[b] Xiaohui Kang,[b,*] Yat-Ming So,[c,*] and Xiaochao Shi[a,*]

[a]*Department of Polymer Materials, School of Materials Science and Engineering, Shanghai University, Materials Building, Nanchen Street 333, Shanghai 200444, China*

[b]*College of Pharmacy, Dalian Medical University, Dalian 116044, China*

[c]*Department of Chemistry, The Hong Kong University of Science and Technology, Hong Kong, China*

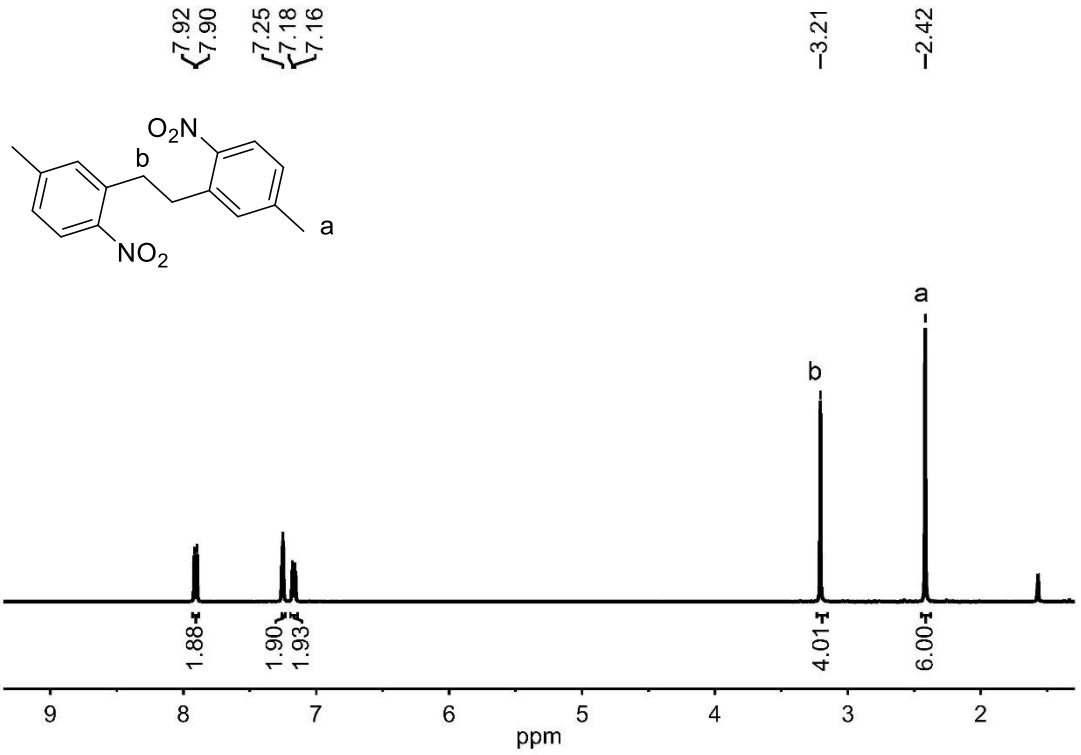

Figure S1 ^{1}H NMR spectrum of 1,2-bis(5-methyl-2-nitrophenyl)ethane. (400 MHz, $CDCl_3$, 25 °C)

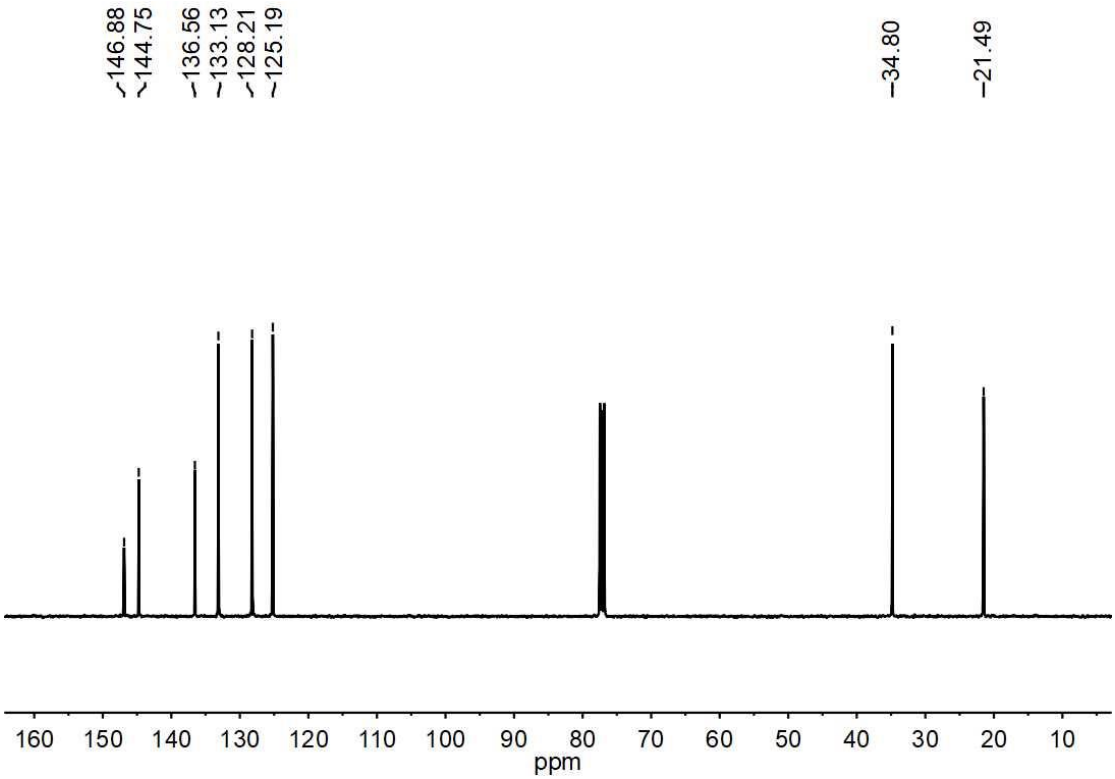

Figure S2 $^{13}C\{^{1}H\}$ NMR spectrum of 1,2-bis(5-methyl-2-nitrophenyl)ethane. (100 MHz, $CDCl_3$, 25 °C)

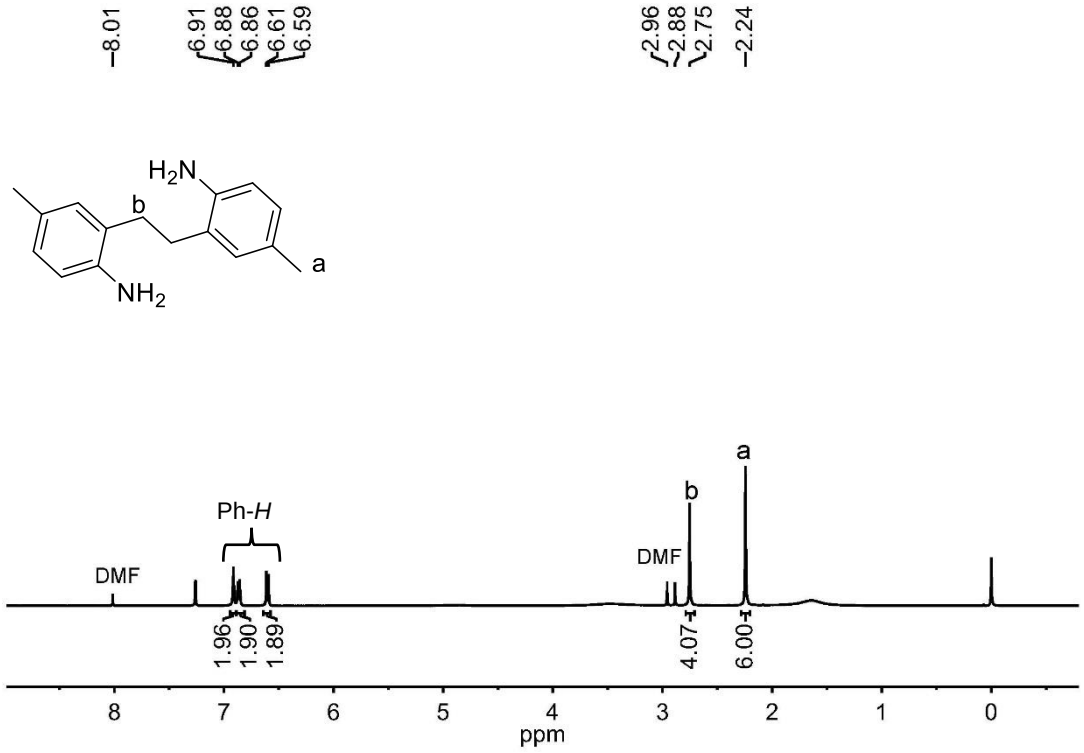

Figure S3 ^{1}H NMR spectrum of 2,2'-(ethane-1,2-diyl)bis(4-methylaniline). (400 MHz, $CDCl_3$, 25 °C)

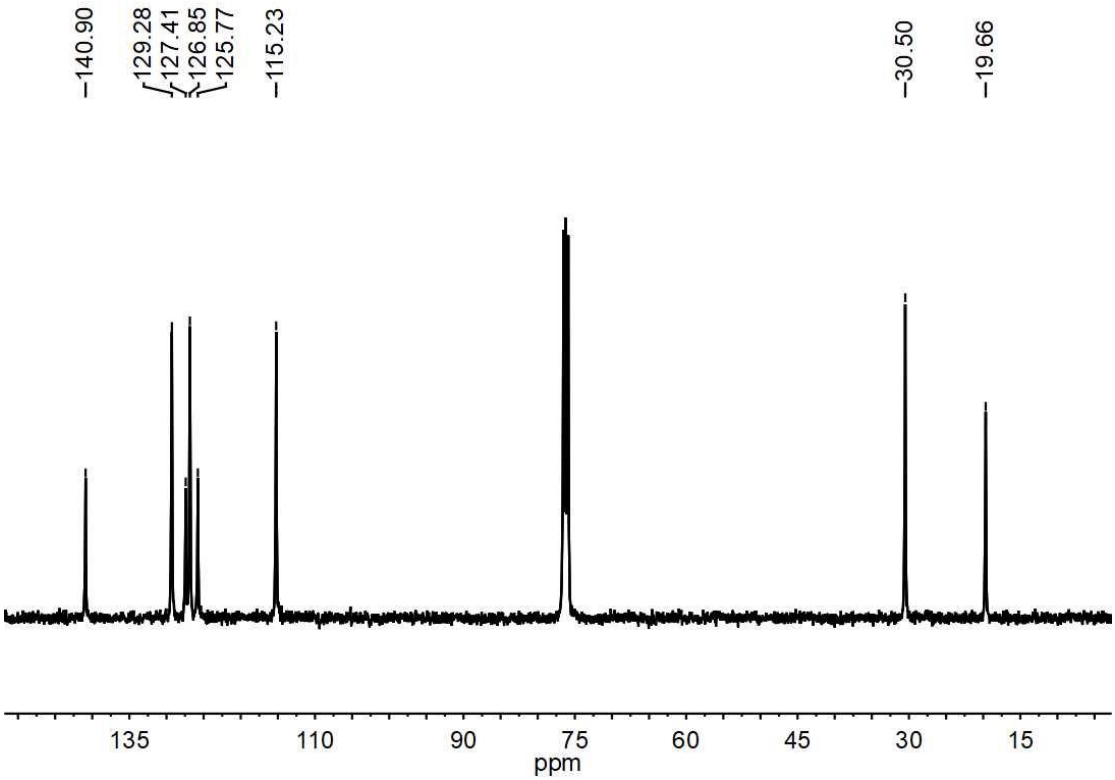

Figure S4 $^{13}C\{^{1}H\}$ NMR spectrum of 2,2'-(ethane-1,2-diyl)bis(4-methylaniline. (100 MHz, $CDCl_3$, 25 °C)

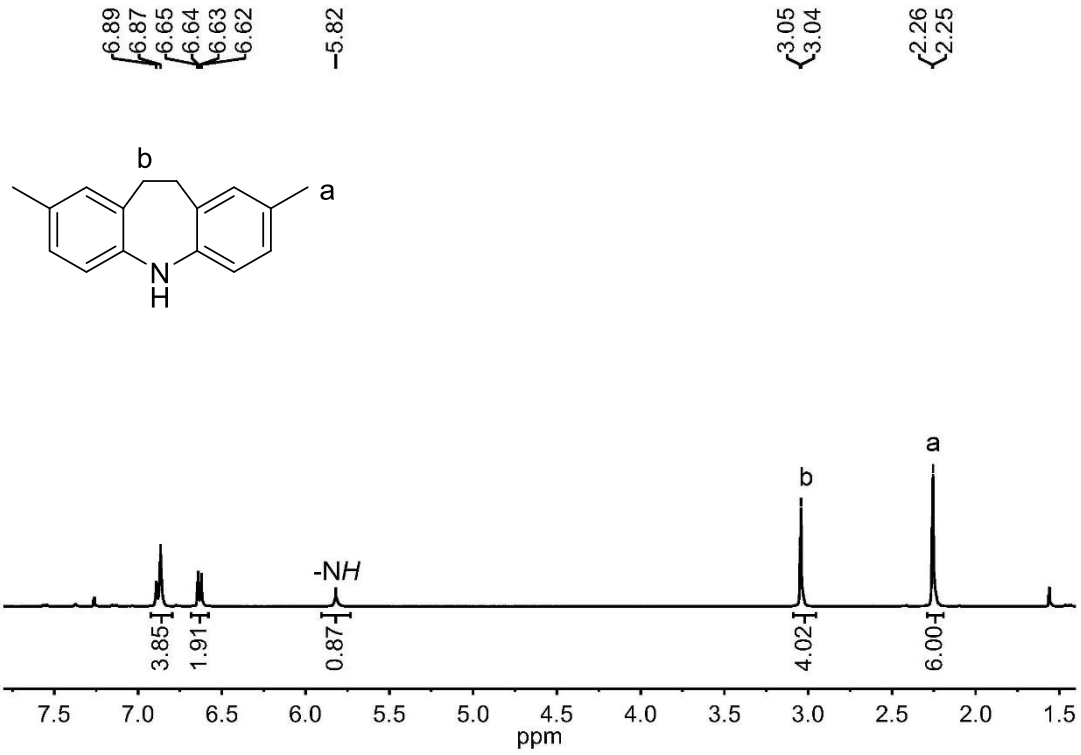

Figure S5 ^{1}H NMR spectrum of ($H[IH_2]$). (400 MHz, $CDCl_3$, 25 °C)

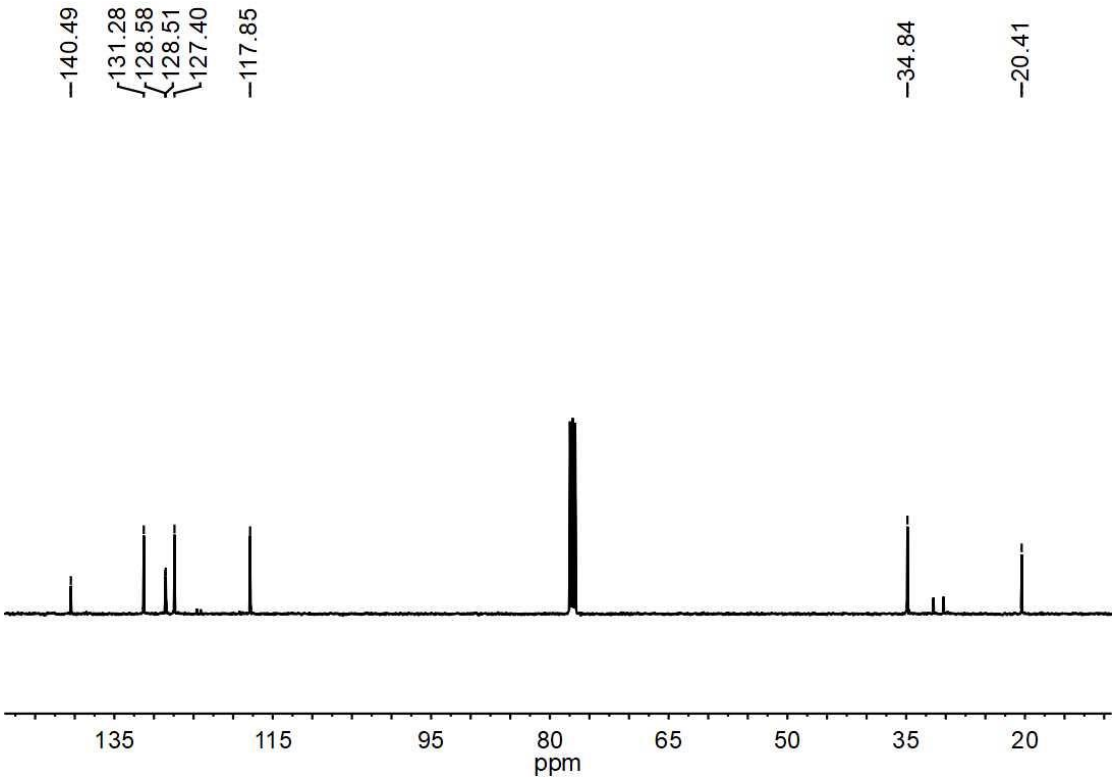

Figure S6 $^{13}C\{^{1}H\}$ NMR spectrum of ($H[IH_2]$). (100 MHz, $CDCl_3$, 25 °C)

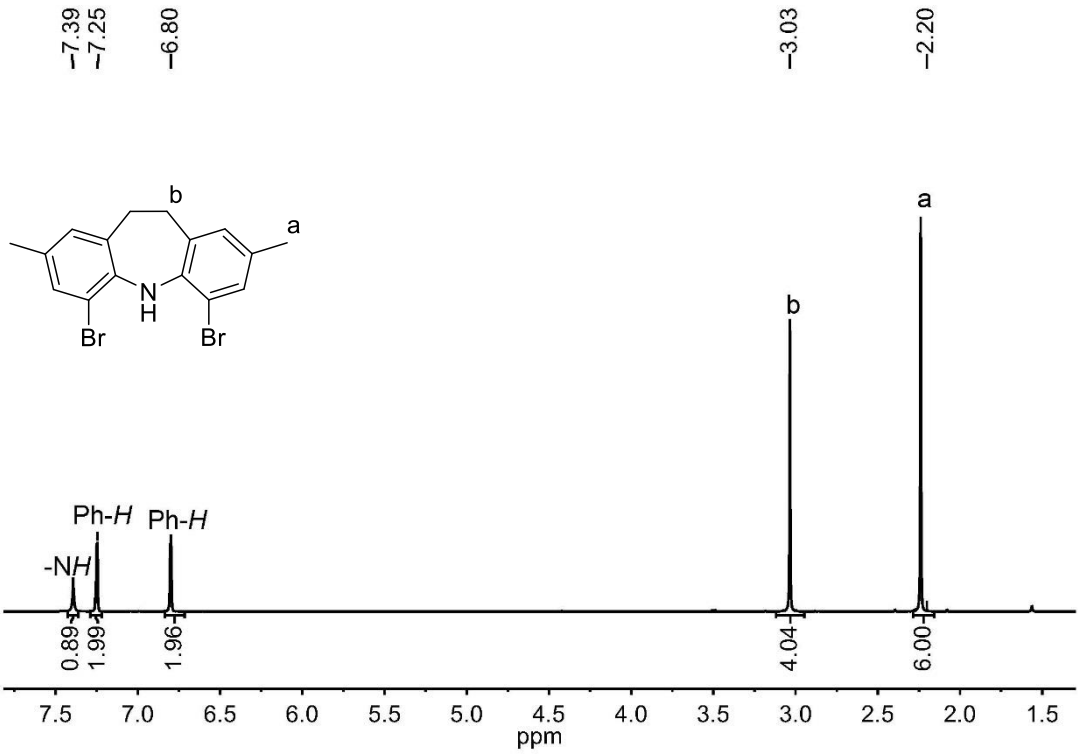

Figure S7 ^{1}H NMR spectrum of ($H[IBr_2]$). (400 MHz, $CDCl_3$, 25 °C)

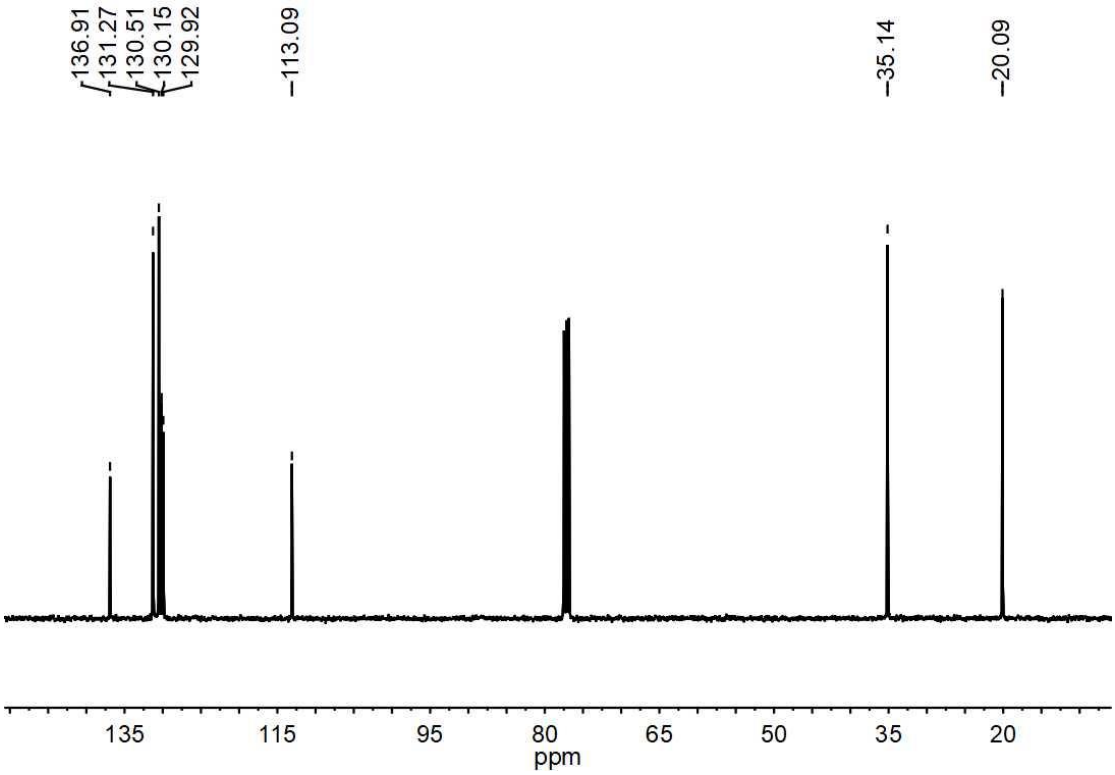

Figure S8 $^{13}C\{^{1}H\}$ NMR spectrum of ($H[IBr_2]$). (100 MHz, $CDCl_3$, 25 °C)

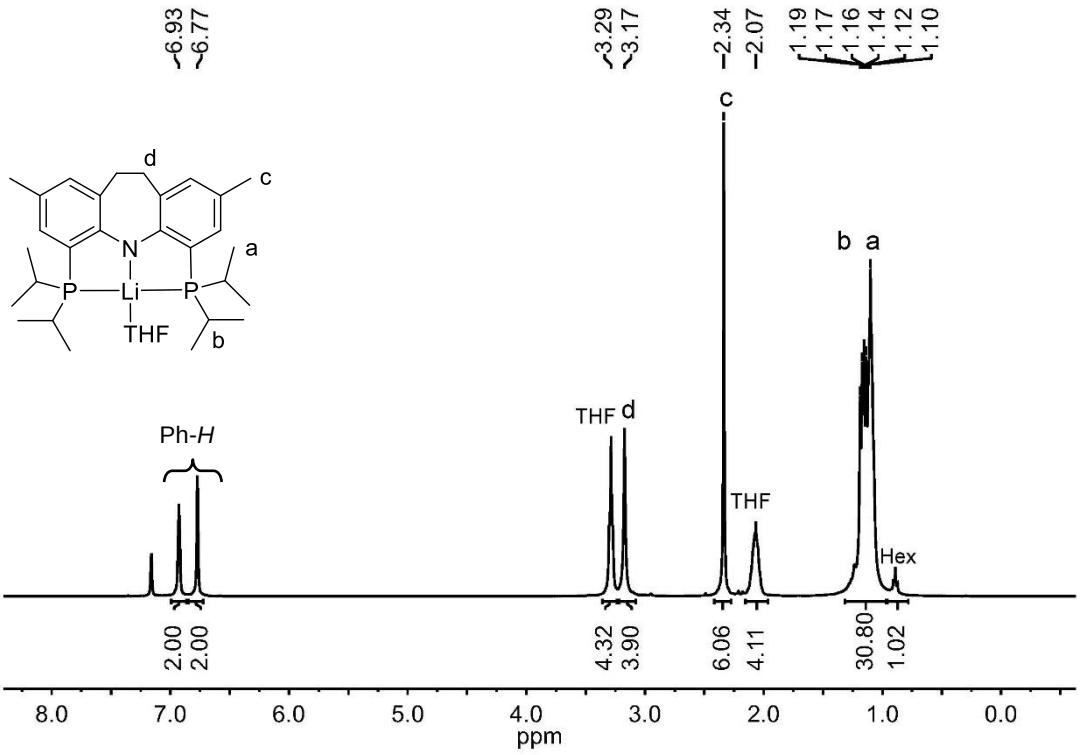

Figure S9 ^{1}H NMR spectrum of ($^{imin\text{-}iPr}$PNP)Li(THF). (400 MHz, C_6D_6, 25 °C)

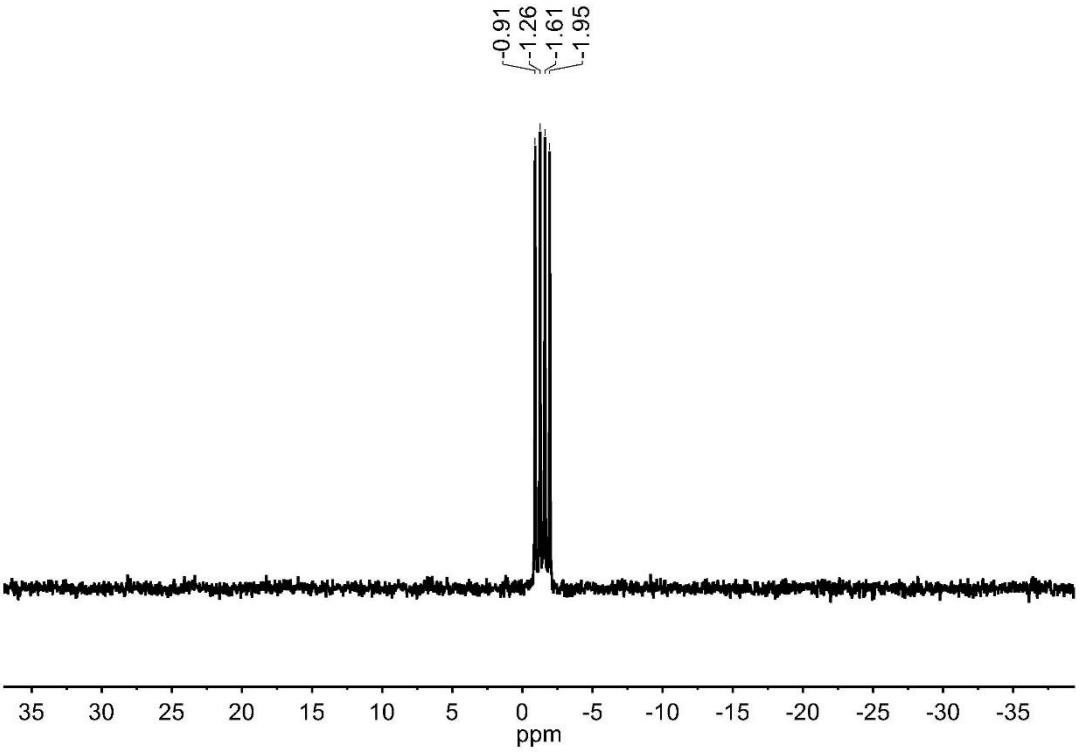

Figure S10 ^{31}P{^{1}H} NMR spectrum of ($^{imin\text{-}iPr}$PNP)Li(THF). (162 MHz, C_6D_6, 25 °C)

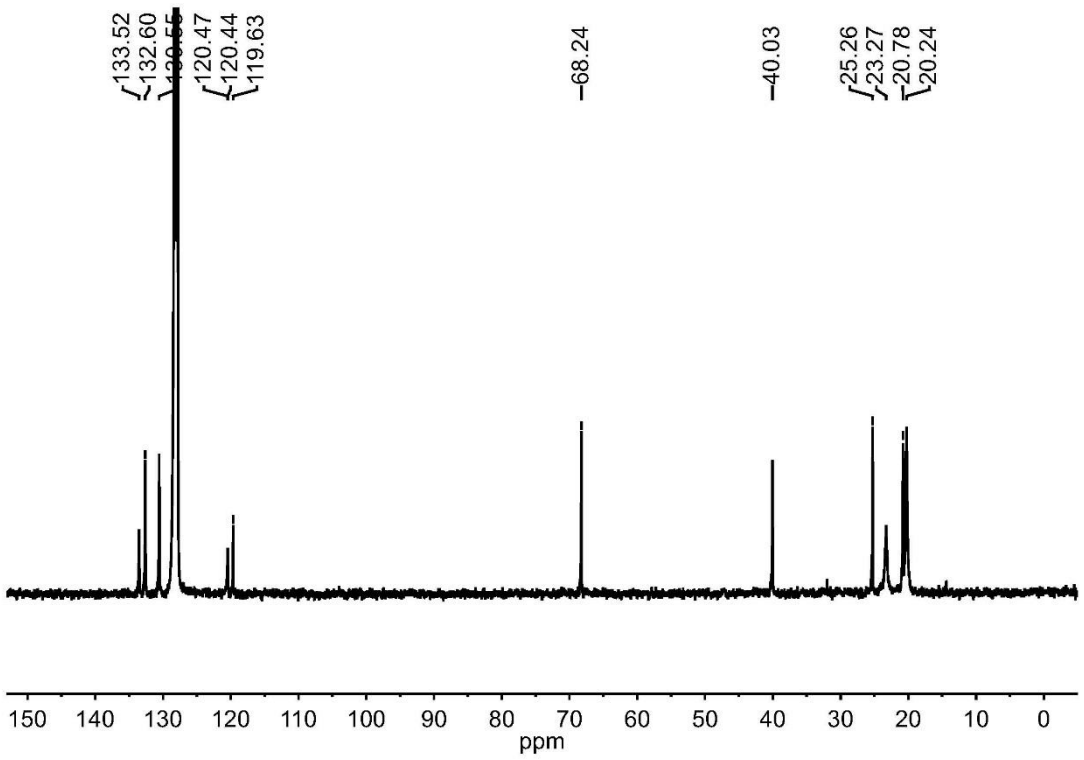

Figure S11 $^{13}C\{^{1}H\}$ NMR spectrum of ($^{imin\text{-}iPr}$PNP)Li(THF). (100 MHz, C_6D_6, 25 °C)

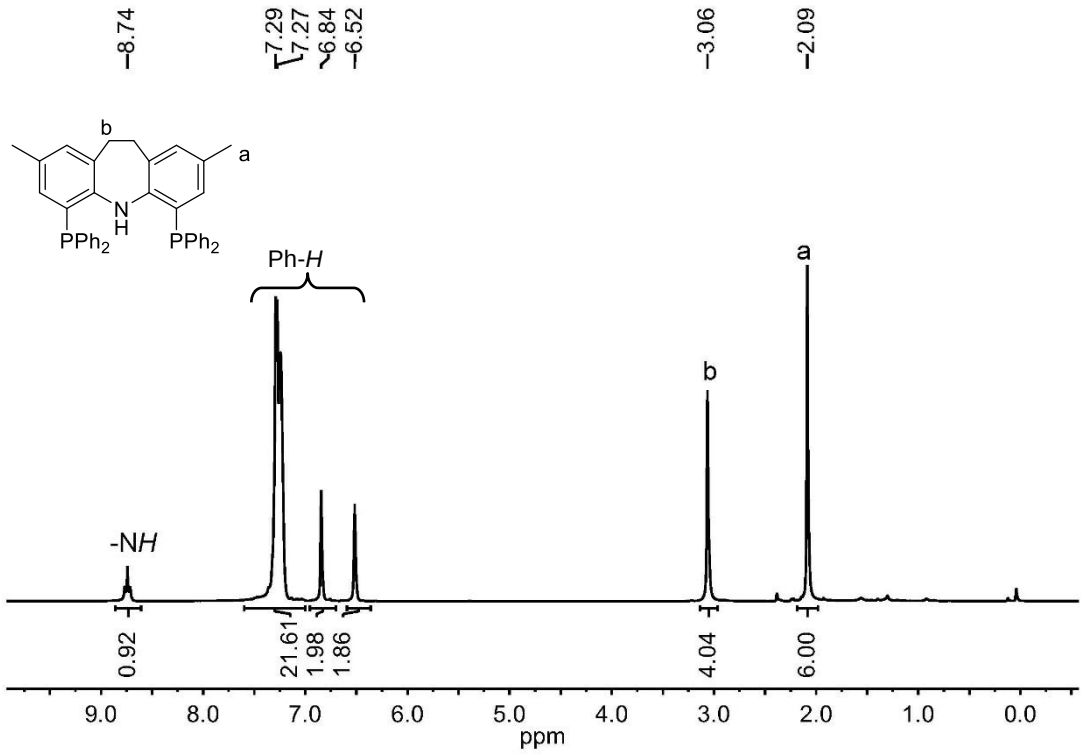

Figure S12 ^{1}H NMR spectrum of $^{imin\text{-}Ph}$PNP. (400 MHz, $CDCl_3$, 25 °C)

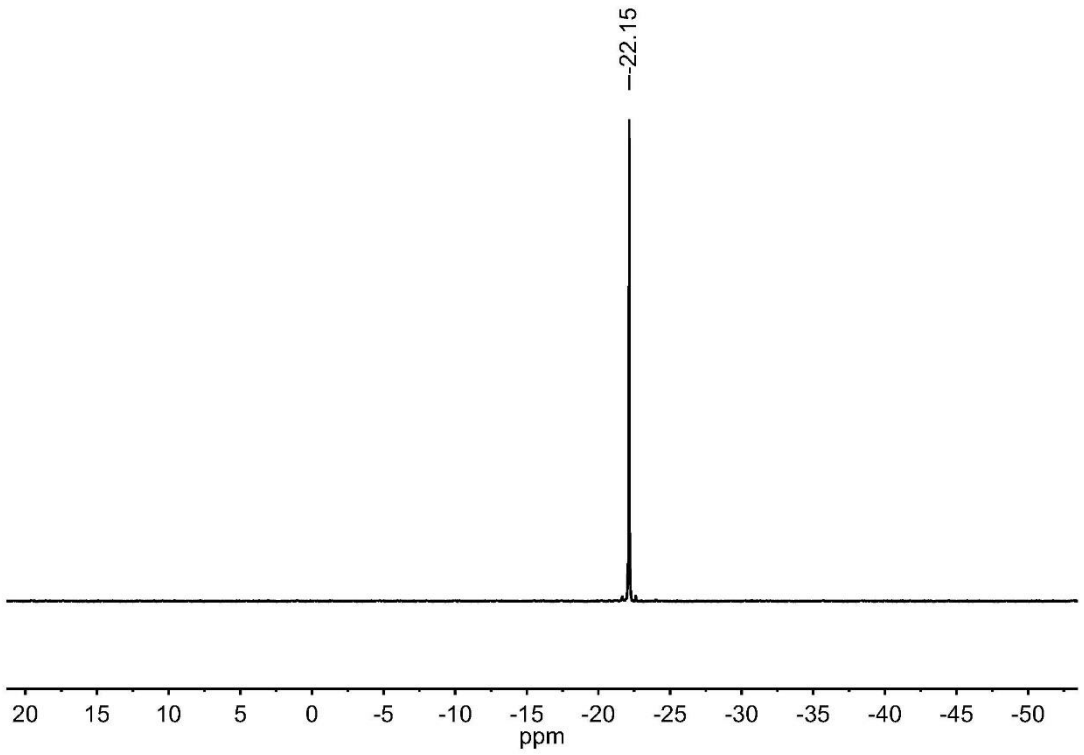

Figure S13 $^{31}P\{^{1}H\}$ NMR spectrum of $^{imin\text{-}Ph}PNP$. (162 MHz, $CDCl_3$, 25 °C)

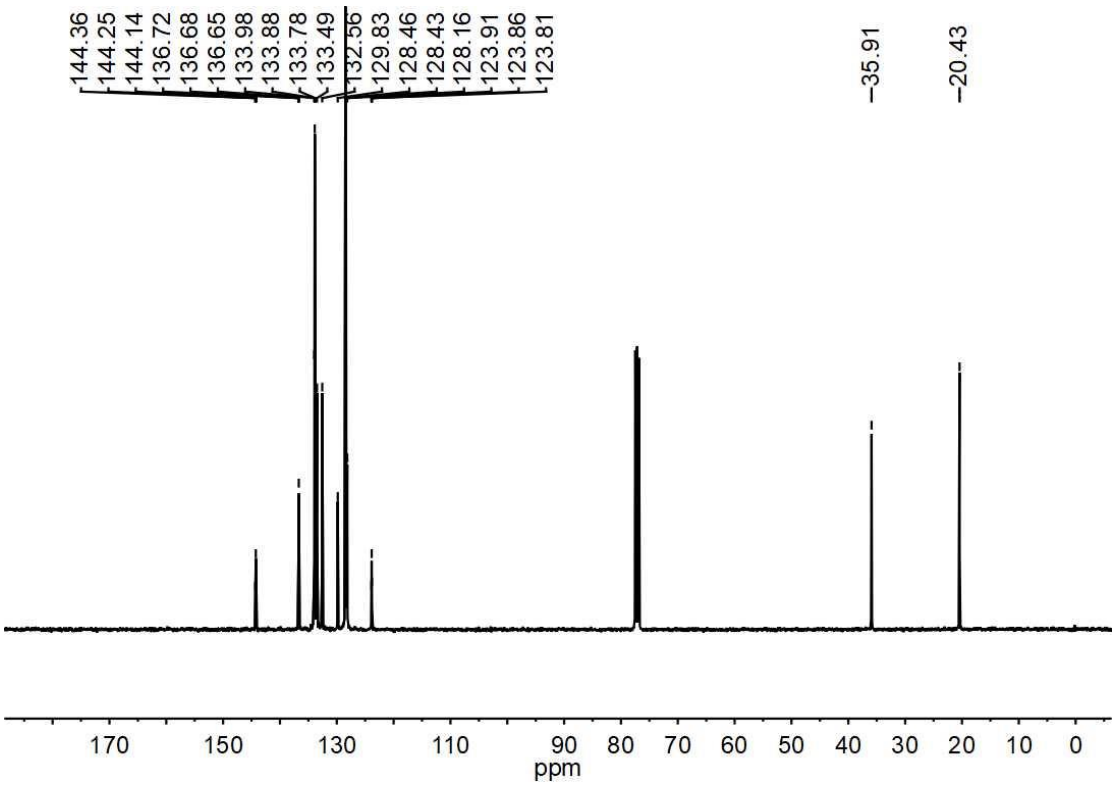

Figure S14 $^{13}C\{^{1}H\}$ NMR spectrum of $^{imin\text{-}Ph}PNP$. (100 MHz, $CDCl_3$, 25 °C)

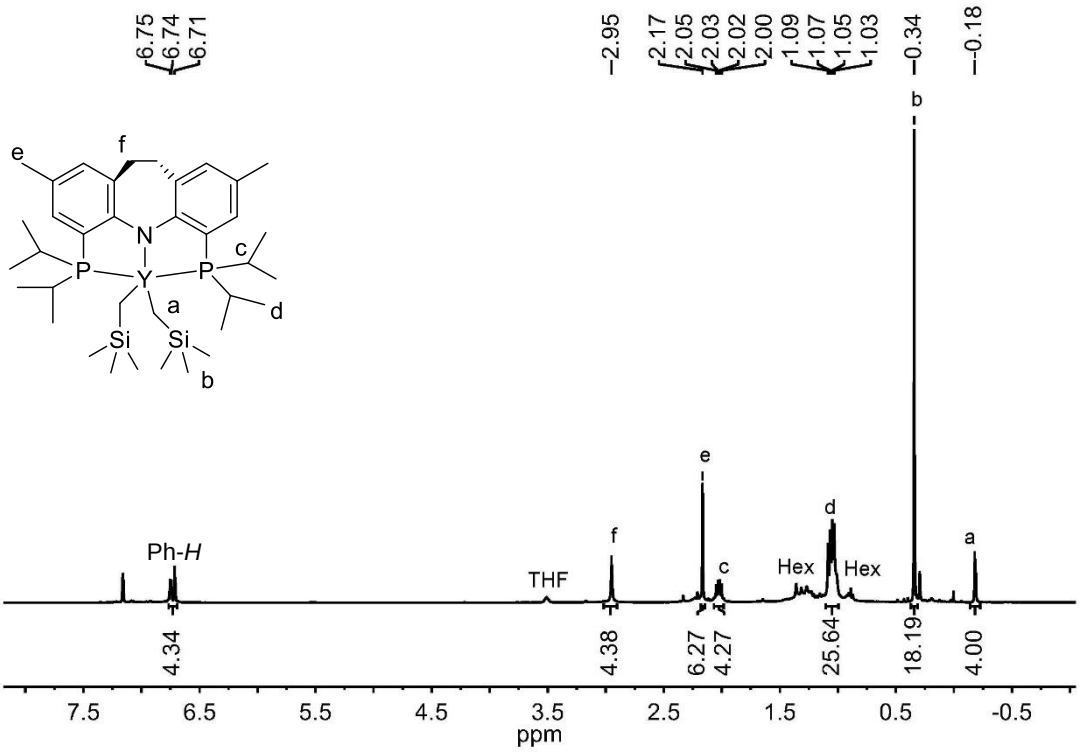

Figure S15 ^{1}H NMR spectrum of ($^{imin\text{-}iPr}$PNP)Y($CH_2SiMe_3)_2$. **(1-Y)** (400 MHz, C_6D_6, 25 °C)

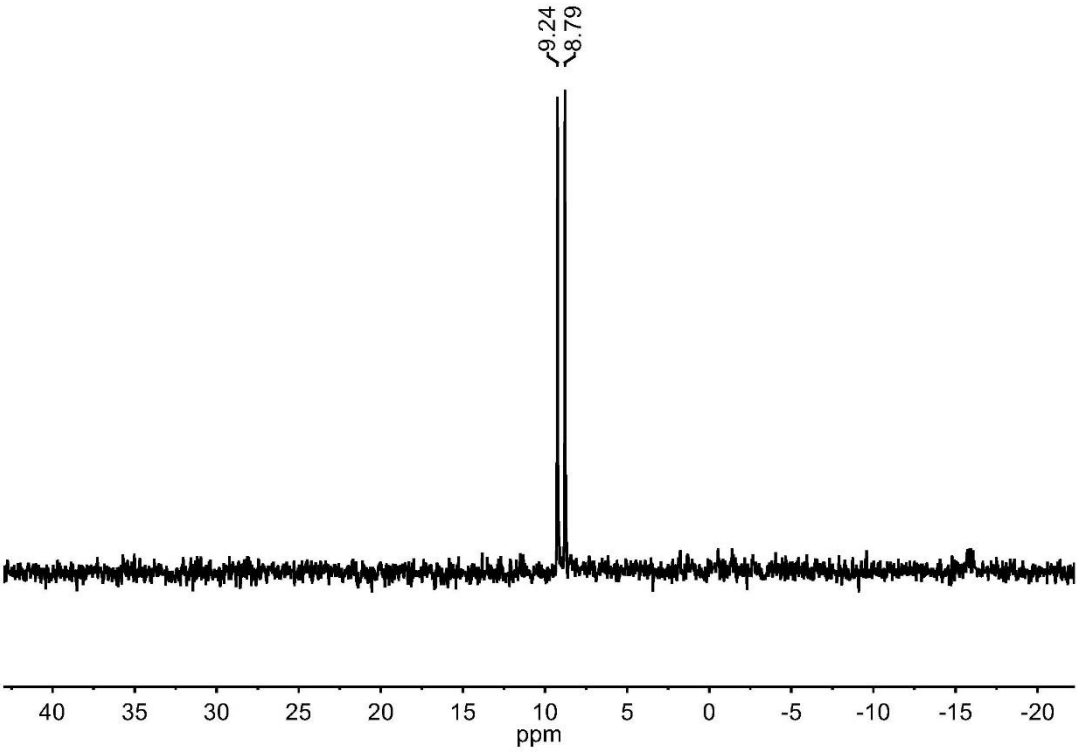

Figure S16 $^{31}P\{^{1}H\}$ NMR spectrum of ($^{imin\text{-}iPr}$PNP)Y($CH_2SiMe_3)_2$. **(1-Y)** (162 MHz, C_6D_6, 25 °C)

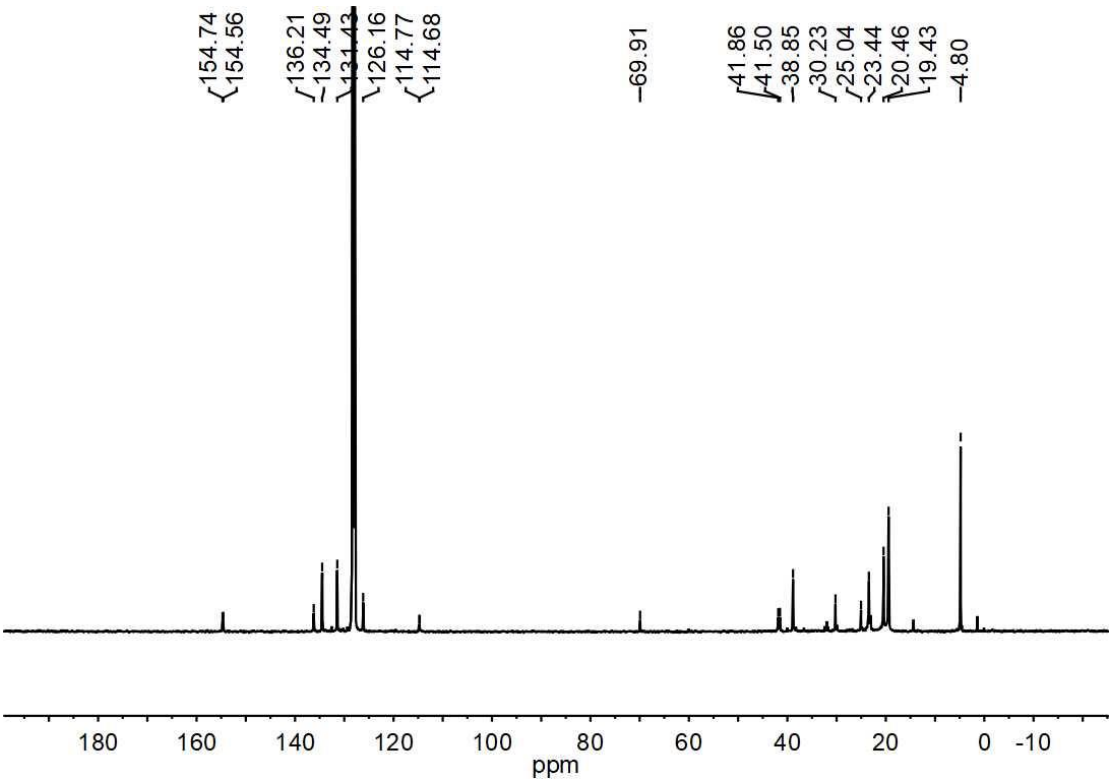

Figure S17 $^{13}C\{^{1}H\}$ NMR spectrum of ($^{imin\text{-}iPr}$PNP)Y(CH_2SiMe_3)$_2$. **(1-Y)** (100 MHz, C_6D_6, 25 °C)

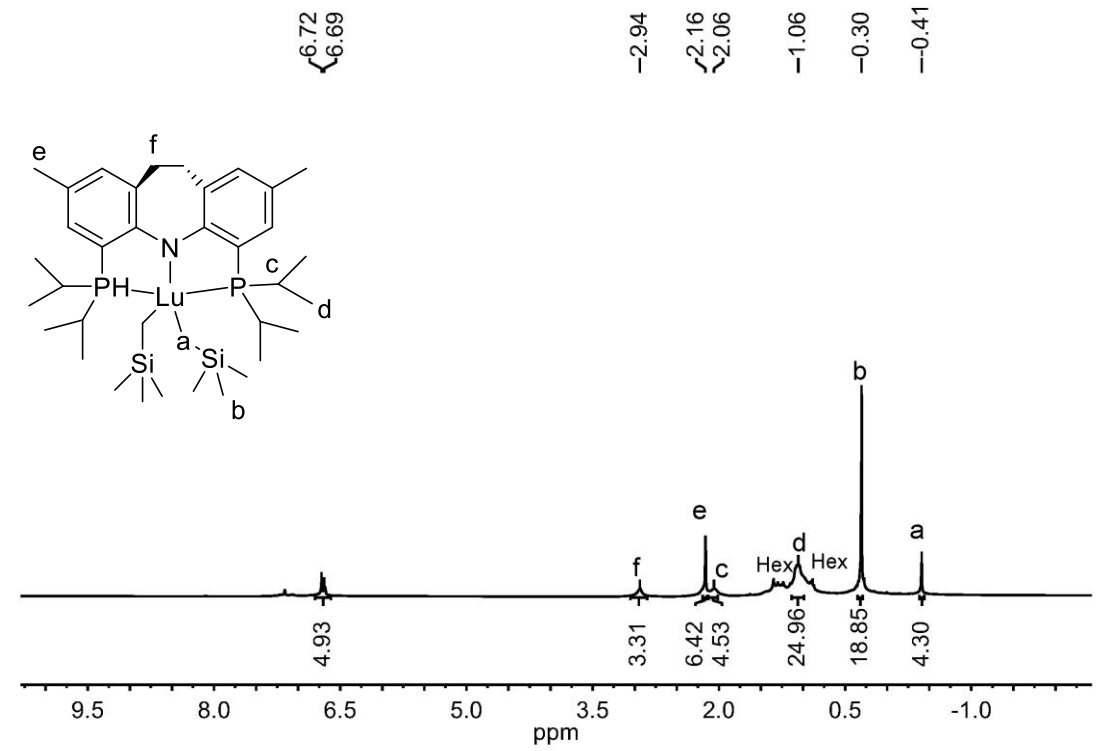

Figure S18 ^{1}H NMR spectrum of ($^{imin\text{-}iPr}$PNP)Lu(CH_2SiMe_3)$_2$. **(1-Lu)** (400 MHz, C_6D_6, 25 °C)

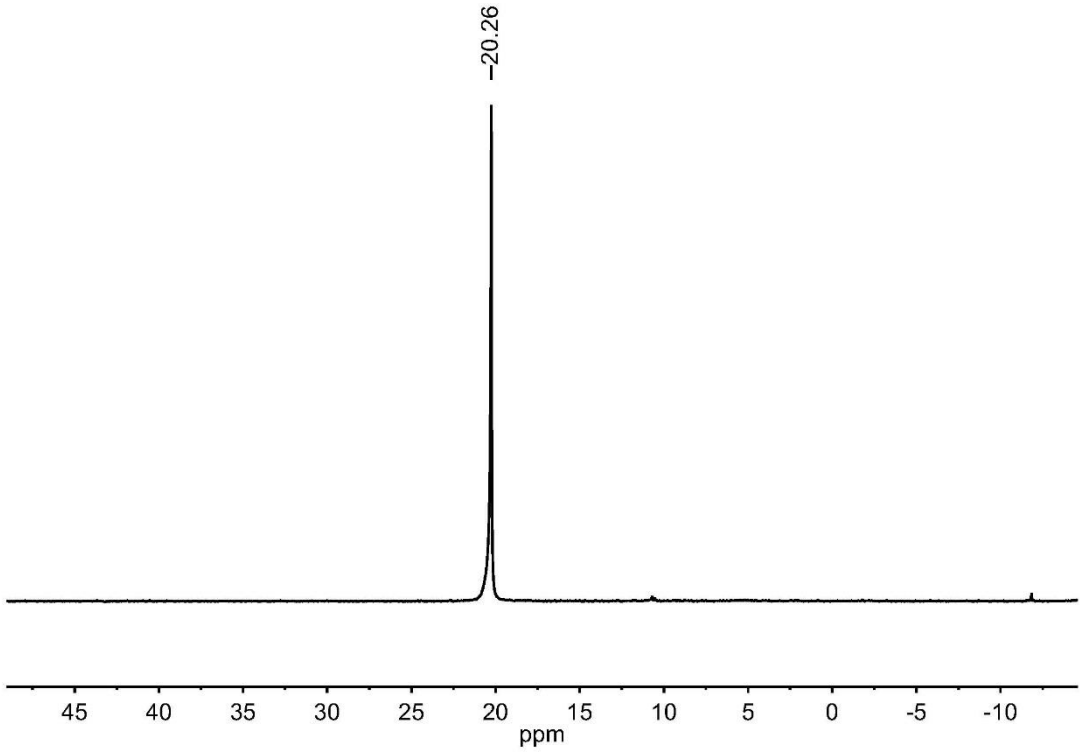

Figure S19 $^{31}P\{^{1}H\}$ NMR spectrum of (($^{imin\text{-}iPr}$PNP)Lu(CH_2SiMe_3)$_2$. **(1-Lu)** (162 MHz, C_6D_6, 25 °C)

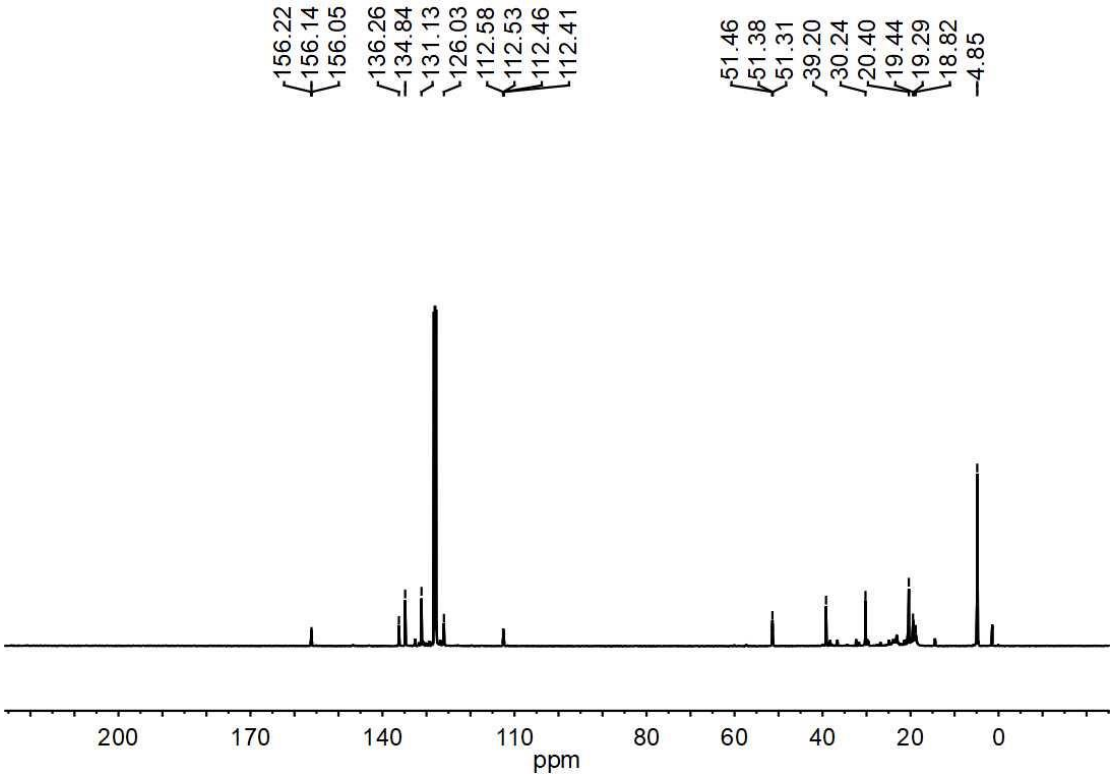

Figure S20 $^{13}C\{^{1}H\}$ NMR spectrum of ($^{imin\text{-}iPr}$PNP)Lu(CH_2SiMe_3)$_2$. **(1-Lu)** (100 MHz, C_6D_6, 25 °C)

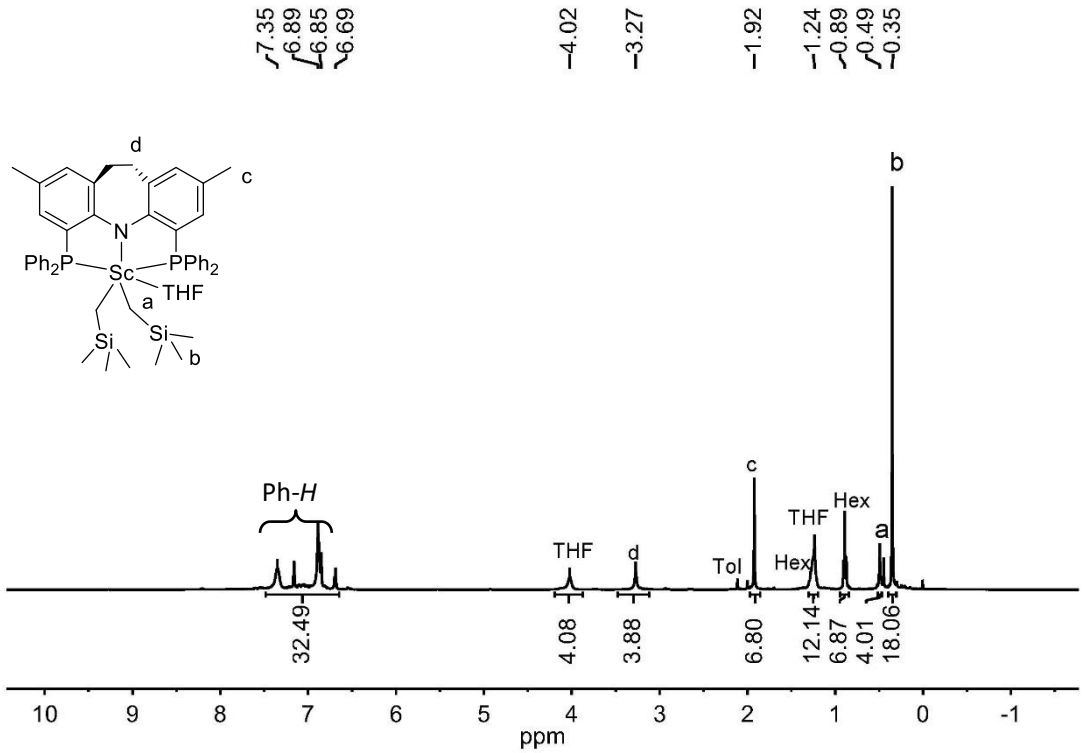

Figure S21 ^{1}H NMR spectrum of ($^{imin\text{-}Ph}$PNP)Sc(CH_2SiMe_3)$_2$. **(2-Sc)** (400 MHz, C_6D_6, 25 °C)

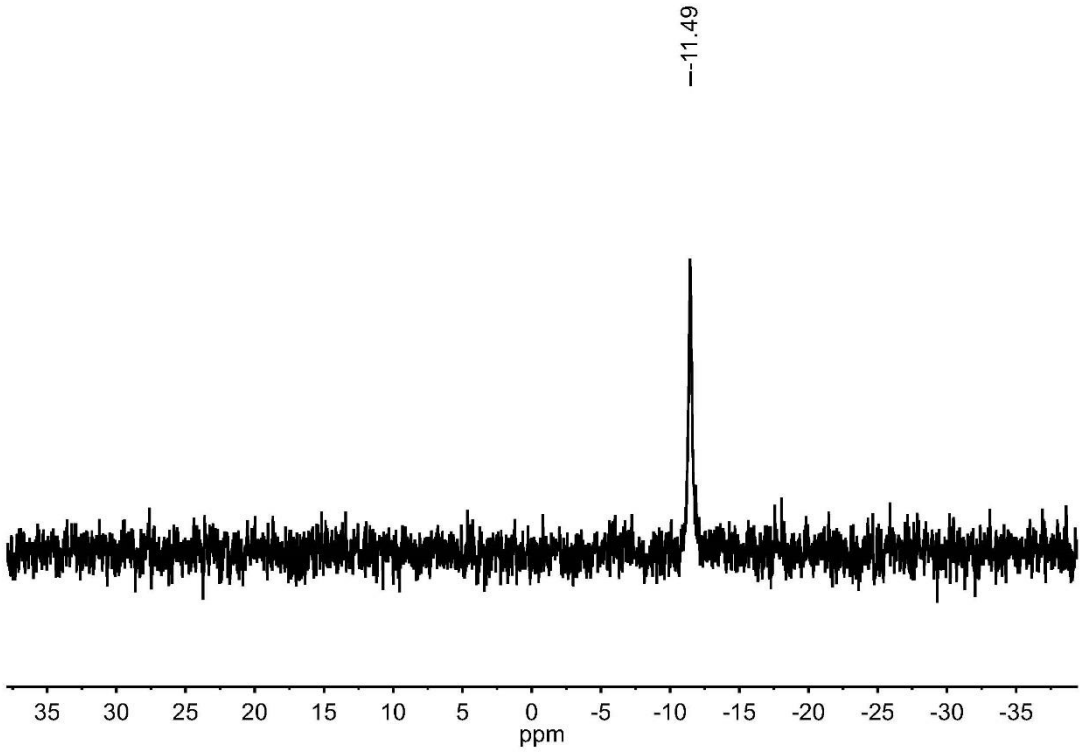

Figure S22 ^{31}P{^{1}H} NMR spectrum of ($^{imin\text{-}Ph}$PNP)Sc(CH_2SiMe_3)$_2$. **(2-Sc)** (162 MHz, C_6D_6, 25 °C)

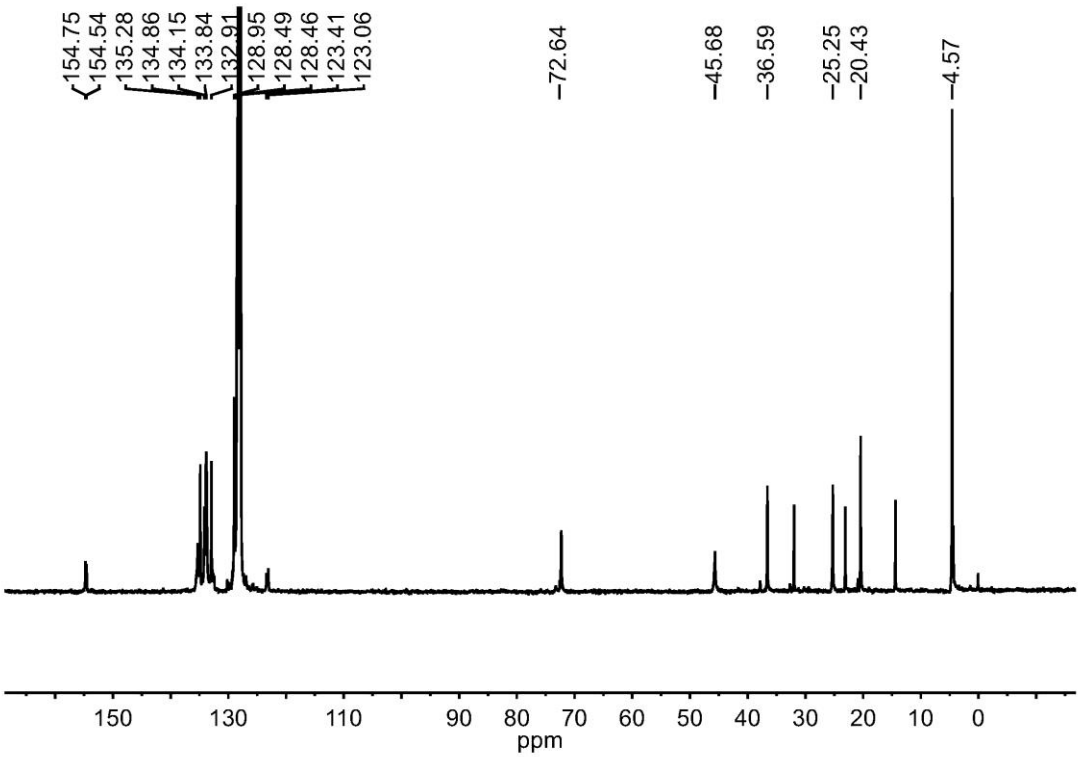

Figure S23 $^{13}C\{^{1}H\}$ NMR spectrum of ($^{imin\text{-}Ph}$PNP)Sc(CH_2SiMe_3)$_2$. **(2-Sc)** (100 MHz, C_6D_6, 25 °C)

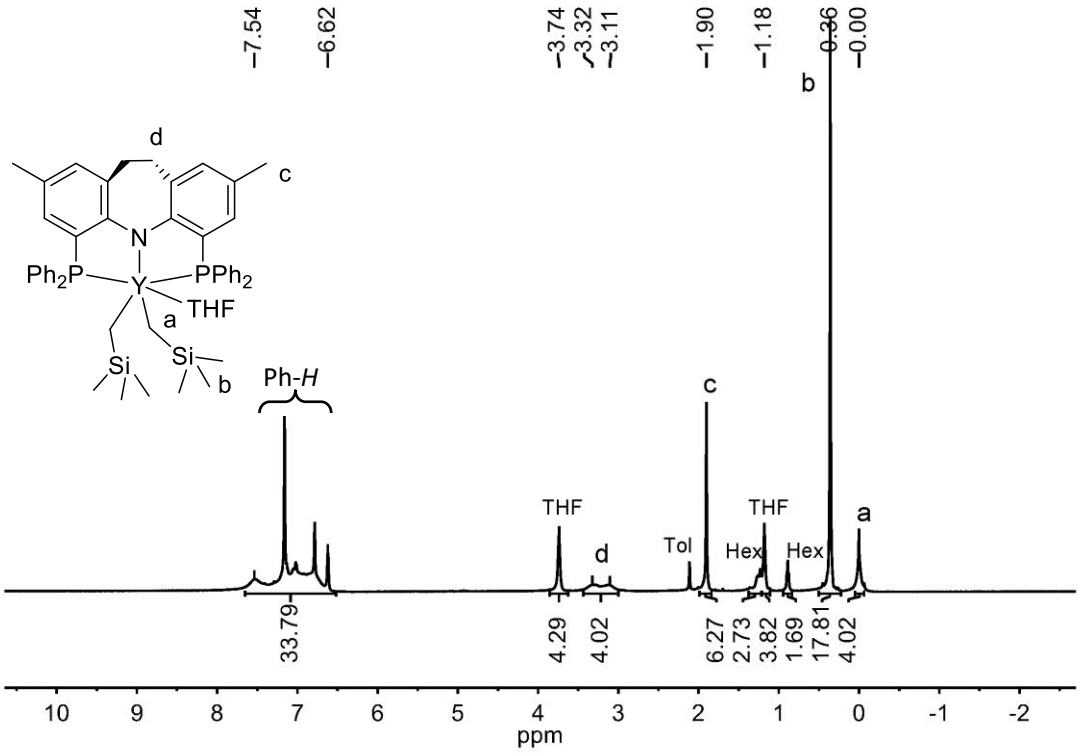

Figure S24 ^{1}H NMR spectrum of ($^{imin\text{-}Ph}$PNP)Y(CH_2SiMe_3)$_2$. **(2-Y)** (400 MHz, C_6D_6, 25 °C)

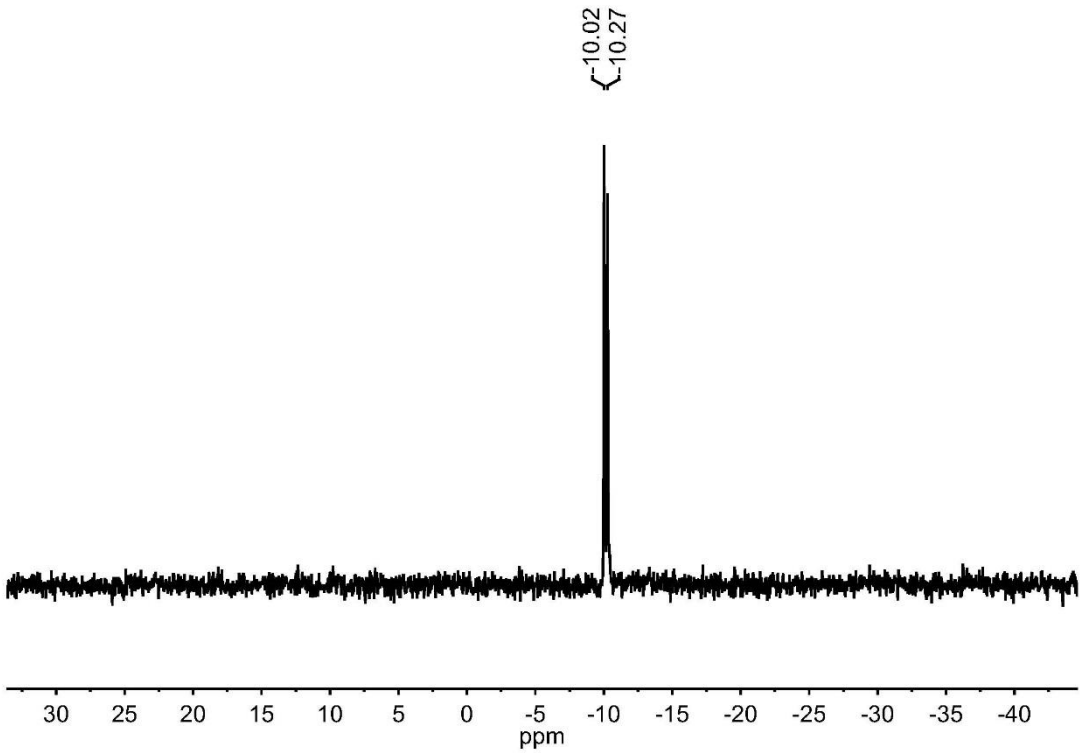

Figure S25 $^{31}P\{^{1}H\}$ NMR spectrum of ($^{imin\text{-}Ph}$PNP)Y(CH_2SiMe_3)$_2$. **(2-Y)** (162 MHz, C_6D_6, 25 °C)

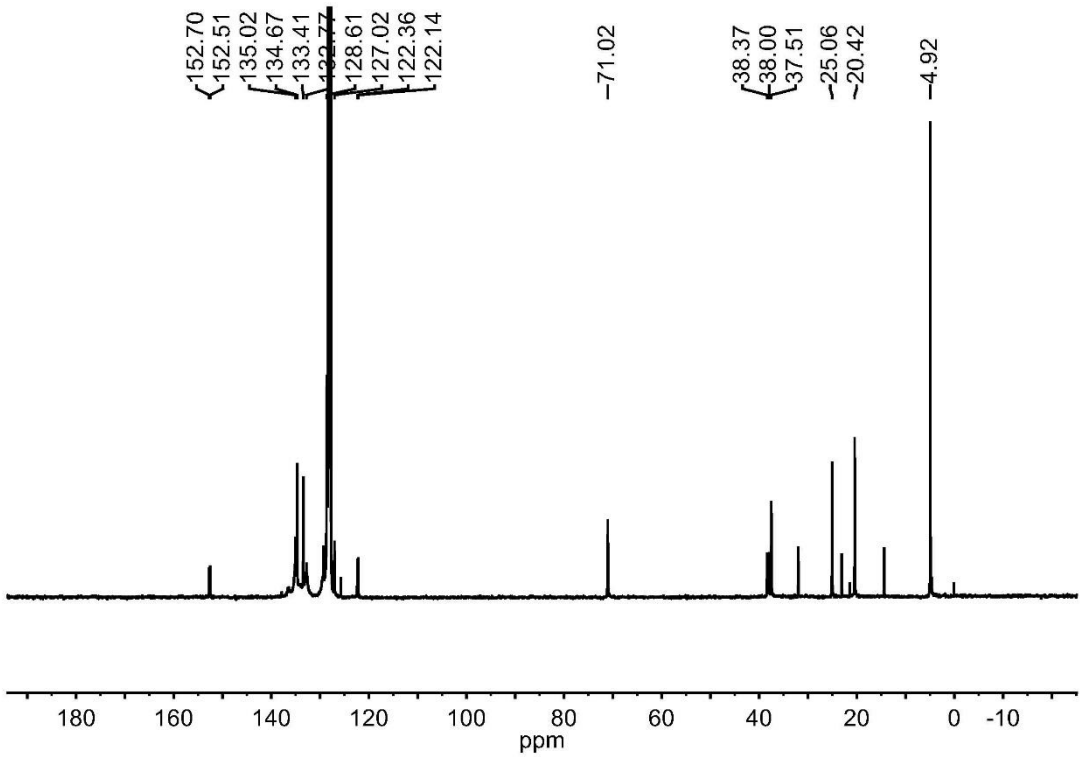

Figure S26 $^{13}C\{^{1}H\}$ NMR spectrum of ($^{imin\text{-}Ph}$PNP)Y(CH_2SiMe_3)$_2$. **(2-Y)** (100 MHz, C_6D_6, 25 °C)

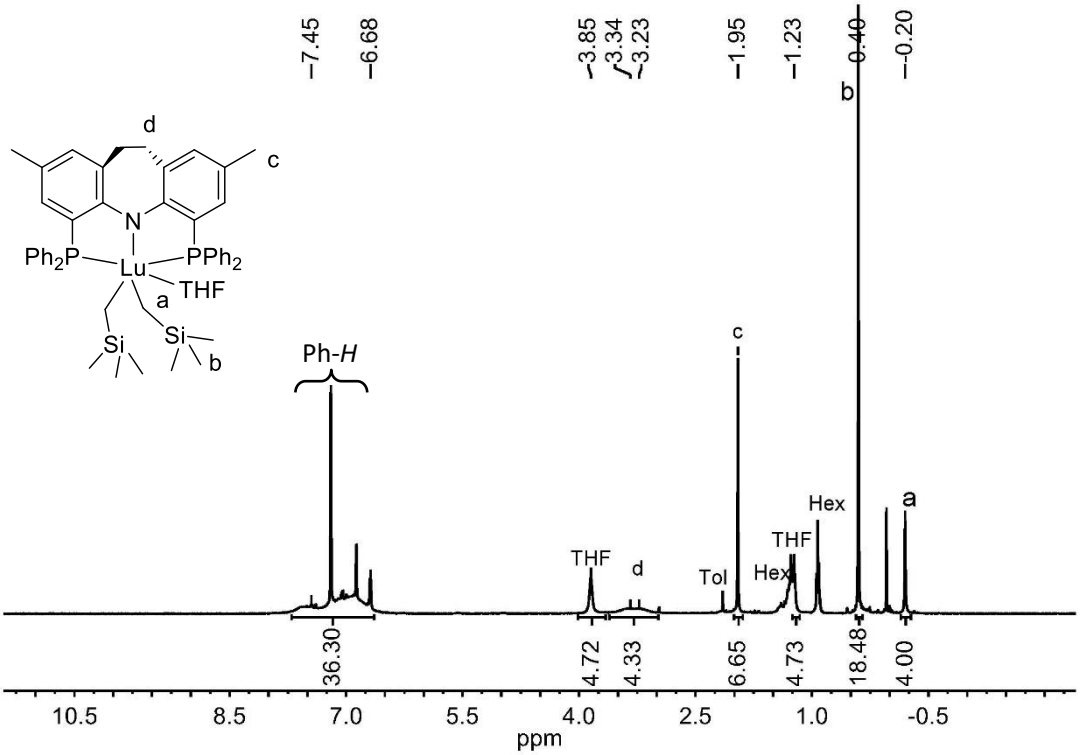

Figure S27 ^{1}H NMR spectrum of ($^{imin\text{-}Ph}$PNP)Lu(CH_2SiMe_3)$_2$. **(2-Lu)** (400 MHz, C_6D_6, 25 °C)

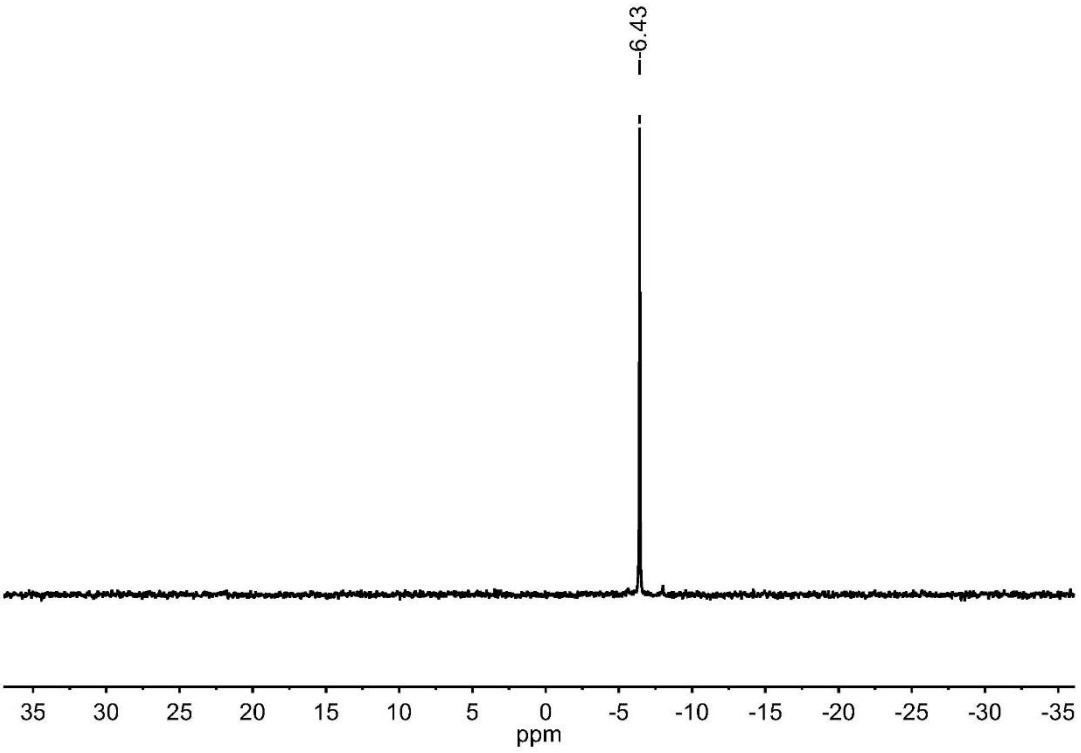

Figure S28 ^{31}P{^{1}H} NMR spectrum of ($^{imin\text{-}Ph}$PNP)Lu(CH_2SiMe_3)$_2$. **(2-Lu)** (162 MHz, C_6D_6, 25 °C)

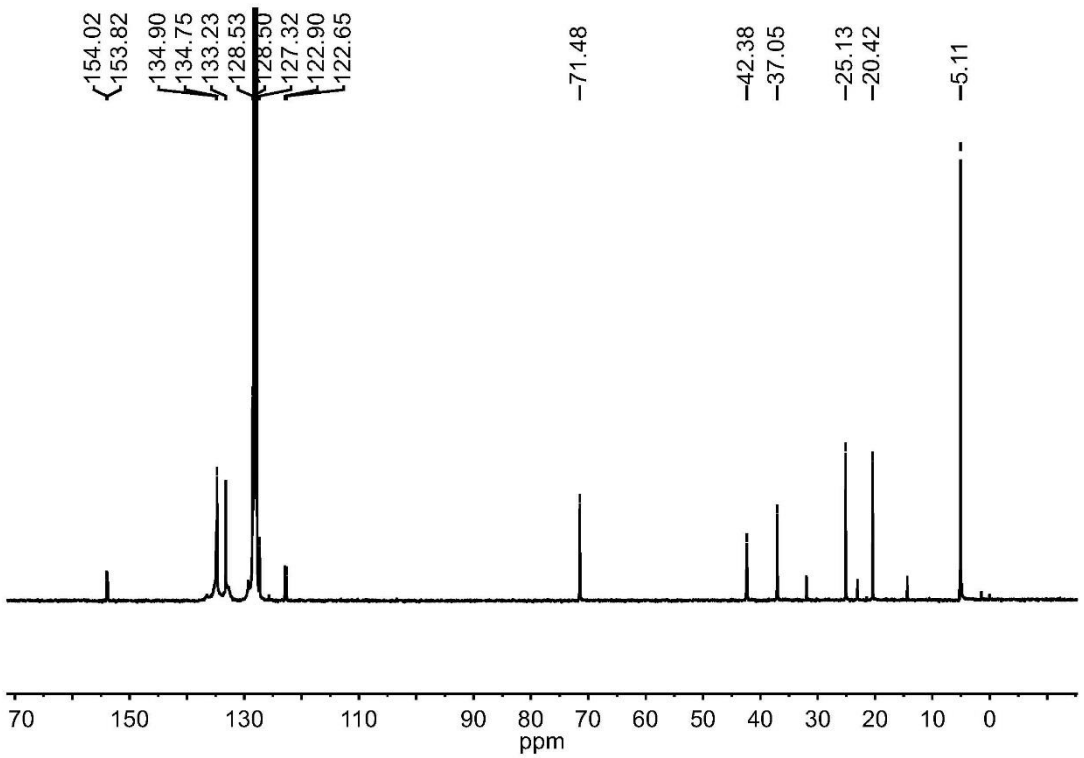

Figure S29 $^{13}C\{^{1}H\}$ NMR spectrum of ($^{imin\text{-}Ph}$PNP)Lu(CH_2SiMe_3)$_2$. **(2-Lu)** (100 MHz, C_6D_6, 25 °C)

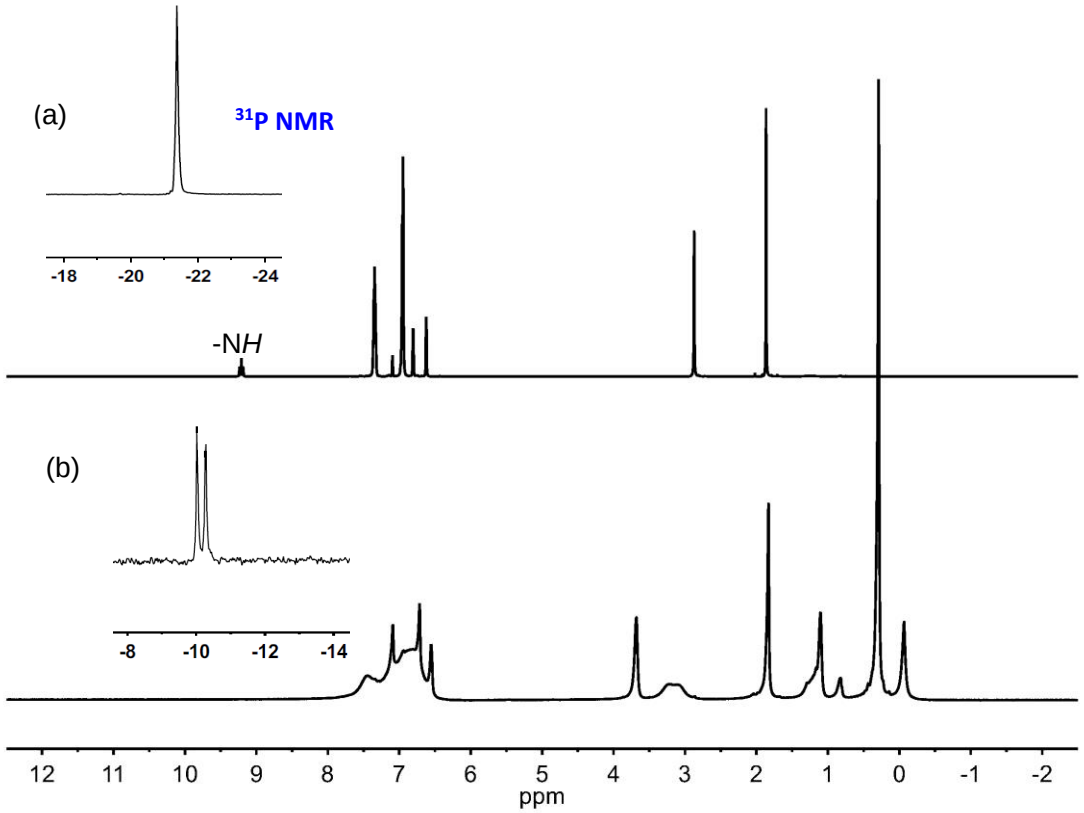

Figure S30 ^{1}H and ^{31}P NMR of $^{imin\text{-}Ph}$PNP (a) and ($^{imin\text{-}Ph}$PNP)Y(CH_2SiMe_3)$_2$ (b). (C_6D_6, 25 °C)

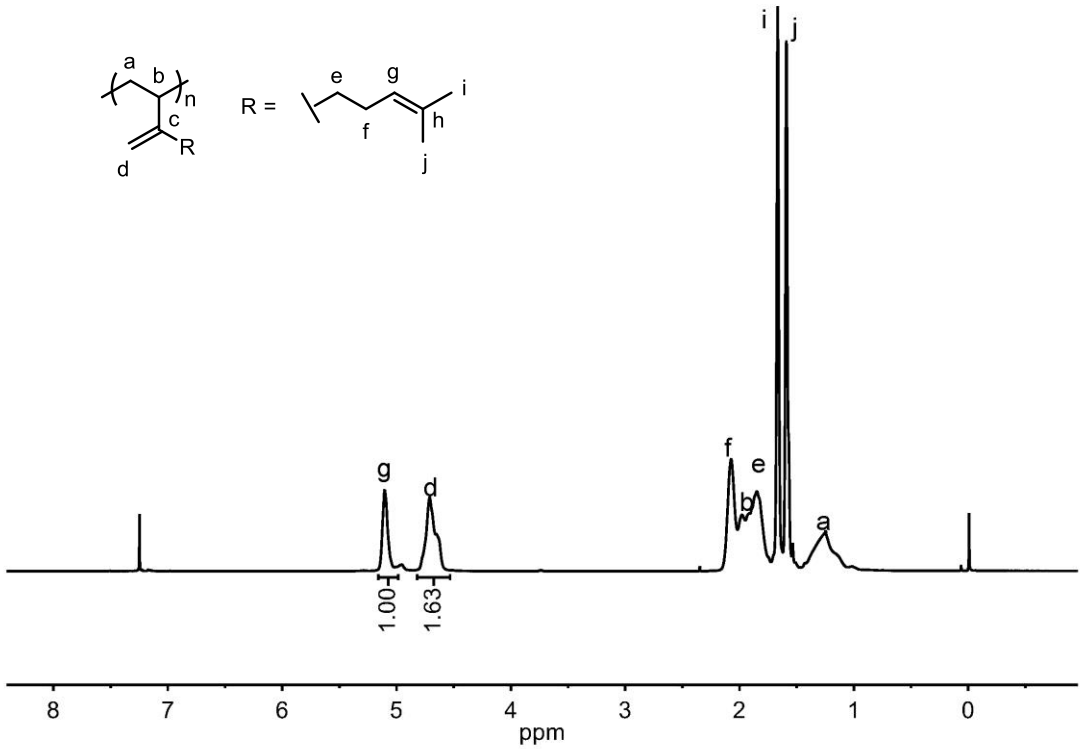

Figure S31 ^{1}H NMR ($CDCl_3$, 25 °C) spectrum of 3,4-selective polymyrcene catalyzed by **2-Y**/[Ph_3C][$B(C_6F_5)_4$]/TIBA (Entry 27 in Table 1).

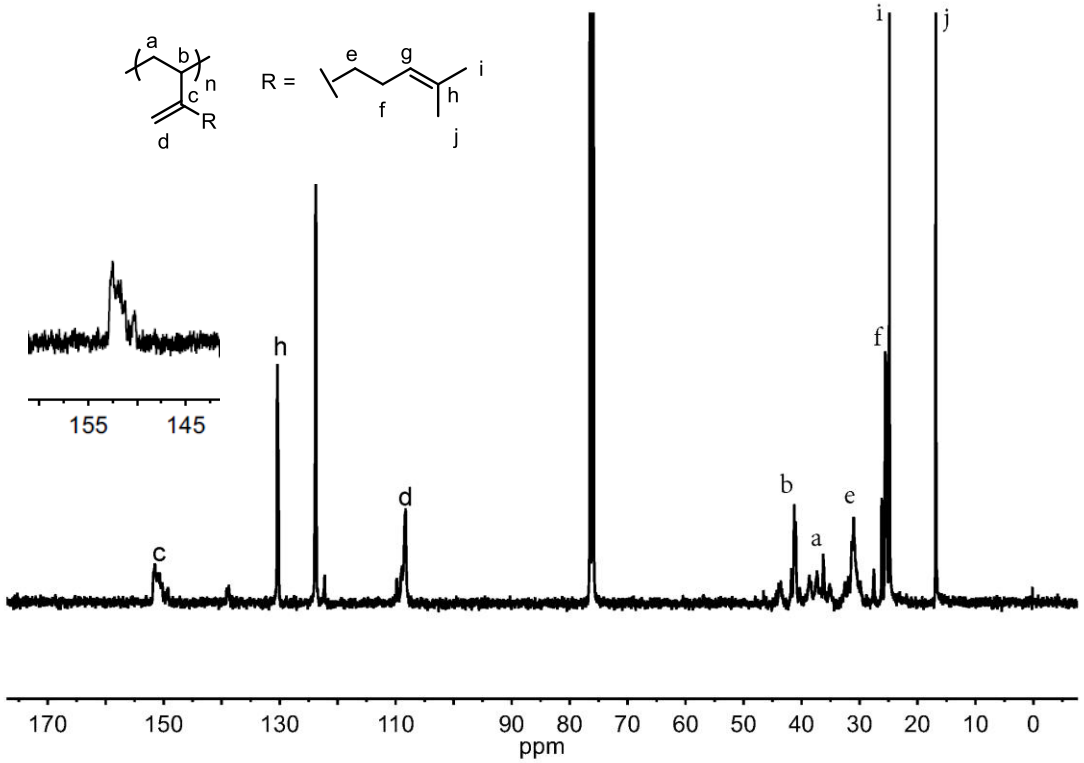

Figure S32 ^{13}C NMR ($CDCl_3$, 25 °C) spectrum of 3,4-selective polymyrcene catalyzed by **2-Y**/[Ph_3C][$B(C_6F_5)_4$]/TIBA (Entry 27 in Table 1).

Computational details

All calculations were performed with Gaussian 16 program.[1] The B3PW91 hybrid exchange-correlation functional was utilized for geometry optimization.[2-4] The 6-31G* basis set was considered for C, H, and N atoms, and the Si, P, and Y atoms were treated by the Stuttgart/Dresden effective core potential (ECP) and the associated basis sets.[5,6] The basis sets of Si and P were augmented with one *d*-polarization function (exponent of 0.284 and 0.387, respectively).[7] This basis set is denoted as "BSI". To obtain more reliable NBO charges, the single-point calculations of optimized structures were carried out at the level of B3PW91-D3 (B3PW91 with Grimme's DFT-D3 correction)[8,9]/BSII, taking into account solvation effect of chlorobenzene with the SMD[10] solvation model. In the BSII, the 6-311G(d,p) basis set was used for nonmetal atoms, while the basis sets together with associated pseudopotentials for Y atom are the same as that in geometry optimization. The buried volume (V_{bur}) were calculated to evalue the steric environment around the active Y center.[11]

(1) Frisch, M. J. T.; G. W.; Schlegel, H. B.; Scuseria, G. E.; Robb, M. A.; Cheeseman, J. R.; Scalmani, G.; Barone, V.; Mennucci, B.; Petersson, G. A.; Nakatsuji, H.; Caricato, M.; Li, X.; Hratchian, H. P.; Izmaylov, A. F.; Bloino, J.; Zheng, G.; Sonnenberg, J. L.; Hada, M.; Ehara, M.; Toyota, K.; Fukuda, R.; Hasegawa, J.; Ishida, M.; Nakajima, T.; Honda, Y.; Kitao, O.; Nakai, H.; Vreven, T.; Montgomery, J. A., Jr.; Peralta, J. E.; Ogliaro, F.; Bearpark, M.; Heyd, J. J.; Brothers, E.; Kudin, K. N.; Staroverov, V. N.; Kobayashi, R.; Normand, J.; Raghavachari, K.; Rendell, A.; Burant, J. C.; Iyengar, S. S.; Tomasi, J.; Cossi, M.; Rega, N.; Millam, N. J.; Klene, M.; Knox, J. E.; Cross, J. B.; Bakken, V.; Adamo, C.; Jaramillo, J.; Gomperts, R.; Stratmann, R. E.; Yazyev, O.; Austin, A. J.; Cammi, R.; Pomelli, C.; Ochterski, J. W.; Martin, R. L.; Morokuma, K.; Zakrzewski, V. G.; Voth, G. A.; Salvador, P.; Dannenberg, J. J.; Dapprich, S.; Daniels, A. D.; Farkas, Ö.; Foresman, J. B.; Ortiz, J. V.; Cioslowski, J.; Fox, D. J. *Gaussian 16, Revision C.01*; Gaussian, Inc.: Wallingford, CT,. **2016**.

(2) Becke, A. Density-functional thermochemistry. III. The role of exact exchange. *J. Chem. Phys.* **1993**, *98*, 5648–5653.

(3) Lee, C.; Yang, W.; Parr, R. Development of the Colic-Salvetti correlation-energy formula into a functional of the electron density. *Phys. Rev. B* **1988**, *37*, 785−789.

(4) Perdew, J.; Burke, K.; Wang, Y. Generalized gradient approximation for the exchange-correlation hole of a many-electron system. *Phys. Rev. B* **1996**, *54*, 16533−16539.

(5) Andrae, D.; H. U.; Dolg, M.; Stoll, H.; P, H. Energy-adjusted Ab initio pseudopotentials for the second and third row transition elements. *Theor. Chim. Acta* **1990**, *77*, 123−141.

(6) Martin, J.; Sundermann, A. Correlation consistent valence basis sets for use with the Stuttgart-Dresden-Bonn relativistic effective core potentials: The atoms Ga-Kr and In-Xe. *J. Chem. Phys.* **2001**, *114*, 3408−3420.

(7) Höllwarth, A.; Böhme, M.; Dapprich, S.; Ehlers, A. W.; Gobbi, A.; Jonas, V.; Köhler, K. F.; Stegmann, R.; Veldkamp, A.; Frenking, G. A set of d-polarization functions for pseudo-potential basis sets of the main group elements Al-Bi and f-type polarization functions for Zn, Cd, Hg, *Chem. Phys. Lett.* **1993**, *208*, 237–240.

(8) Grimme, S.; Antony, J.; Ehrlich, S.; Krieg, H. A consistent and accurate ab initio parametrization of density functional dispersion correction (DFT-D) for the 94 elements H-Pu. *J. Chem. Phys.* **2010**, *132*, 154104–15424.
(9) Grimme, S. Accurate description of van der waals complexes by density functional theory including empirical corrections. *J. Comput. Chem.* **2004**, *25*, 1463–1473.
(10) Marenich, A.; Cramer, C.; Truhlar, D. Universal solvation model based on solute electron density and on a continuum model of the solvent defined by the bulk dielectric constant and atomic surface tensions. *J. Phys. Chem. B.* **2009**, *113*, 6378–6396.
(11) Falivene, L.; Cao, Z.; Petta, A.; Serra, L.; Poater, A.; Oliva, R.; Scarano, V.; Cavallo, L. Towards the online computer-aided design of catalytic pockets, *Nat. Chem.* **2019**, *11*, 872–879.